Journal of Marine Research, 62, 517–543, 2004

Baroclinic boundary currents with downstream decreasing buoyancy: A study of an idealized Nordic Seas system

by Gösta Walin[1], Göran Broström[2,3], Johan Nilsson[2] and Olof Dahl[1]

ABSTRACT

The dynamics of a baroclinic boundary current losing buoyancy along its path is analyzed both theoretically and using a numerical ocean-circulation model. A fundamental ingredient in our analysis is that the side boundaries of the ocean basin are sloping gently down to the deep ocean. Theoretically we find that the coastal boundary current develops two branches: one seaward baroclinic jetstream and one barotropic current, which is confined to the continental slope. The baroclinic jetstream decreases its transport as the buoyancy is lost from the surface layer. This decrease in transport is compensated by an increase in the barotropic flow on the slope. When the buoyancy is lost altogether, the entire volume transport occurs in the barotropic slope current.

In our numerical experiments we focus on the penetration of warm water over a sill into a cold semi-enclosed basin. The flow enters as a baroclinic current with a thickness approximately equal to the sill depth and proceeds around the basin on essentially the same depth while being transformed to a barotropic slope current which leaves the basin over the sill. It should be noted that the circulation does not involve any renewal of the deep water in the cold basin, except in the initial spin up of the system.

We suggest that our results can illuminate some basic aspects of the dynamics in the Nordic Seas, which are invaded by North Atlantic surface water over the Greenland-Scotland Ridge. One striking example; is the observations reported by Orvik *et al.* (2001), which show that the flow of Atlantic water along the Norwegian coast has two branches: A baroclinic jetstream and a shelf-bound barotropic current. The existence of this double-flow structure is to be expected from our theoretical considerations and numerical simulations.

1. Introduction

We will consider the dynamics of a layer of buoyant water flowing along a coast while losing its buoyancy. This study is, to a great extent, inspired by the conditions in the Nordic Seas; i.e., the ocean north of the Greenland-Scotland Ridge (see Fig. 1). In particular, we have in mind the conditions along the Norwegian coast where the northern-most branch of the North Atlantic Current dominates the oceanographic conditions; see Mauritzen (1996)

1. Department of Oceanography, Earth Sciences Center, Göteborg University, Box 460, SE-40530 Göteborg, Sweden.
2. Department of Meterology, Stockholm University, SE 10691, Stockholm, Sweden.
3. Corresponding author: ***email: goran@misu.su.se***

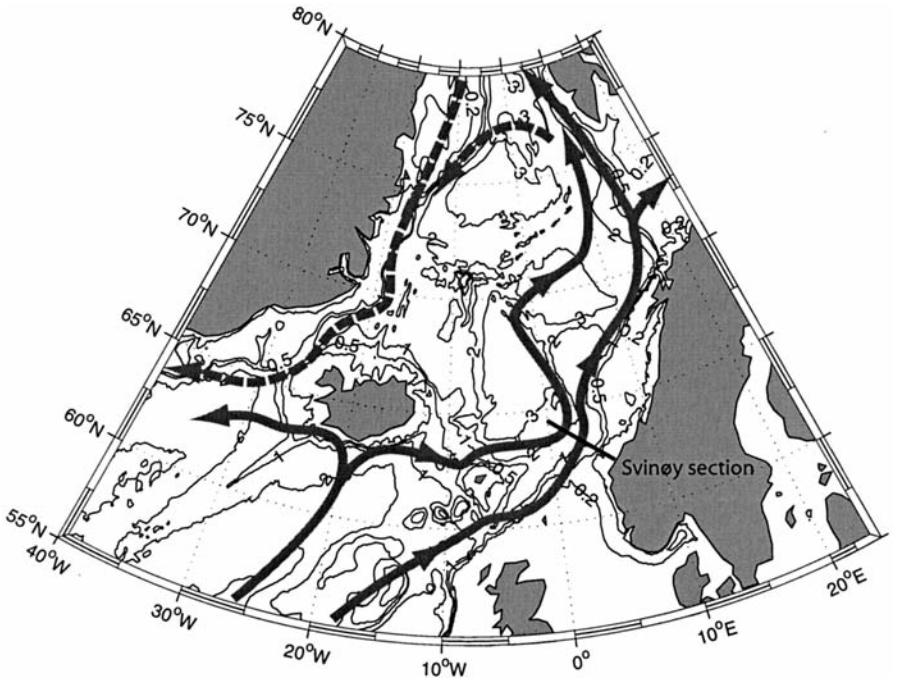

Figure 1. A schematic of the main pathways of the Atlantic water in the Nordic Seas (see also Orvik and Niiler, 2002). The solid/dashed lines represent warm/cold Atlantic water. The Svinøy section is marked, where the shoreward Atlantic branch is known as the Norwegian Slope Current. Note that the size of the arrows does not correspond to transport magnitudes and that the transfer between the main branches is not depicted.

and Hansen and Østerhus (2000) for an overview. The possible relevance of our analysis for the dynamics in this region will be considered in the last section.

a. Some aspects on buoyant coastal currents

A buoyant coastal current forms when the surface layer in the near-shore region is less dense than the water farther offshore. In the northern hemisphere the surface layer moves to the right relative to the underlying water, when looking away from the coast. The accumulation of light water along the coast may be created in different ways. The reason may be a supply of freshwater from rivers which creates a brackish layer, or wind forcing, which accumulates buoyant surface water along the coast.

The baroclinic exchange of water masses between ocean basins having different densities may also create buoyant coastal currents. Such exchange involves dense and light water flowing in opposite directions through a constriction between the basins. Inside the basin containing the dense water, the light water generally forms a buoyant boundary current that may penetrate a considerable distance along the coast. A prominent example is

the Nordic Seas, where the warm Atlantic water flows northward along the Norwegian coast (Orvik *et al.,* 2001). A similar buoyant current is also formed when the brackish water from the Baltic Sea flows through Kattegatt (Rodhe, 1998).

The volume transport in a coastal current can be calculated if the deep water motions underneath are either known or small compared with the velocities in the buoyant layer. In the special case when the buoyant layer is essentially homogeneous and the thickness of the layer vanishes altogether at some distance from the coast, the volume transport M may be calculated from the geostrophic balance (see, e.g., Stommel, 1966, p. 111)

$$M = \frac{g\Delta\rho H^2}{2f\rho_0}, \tag{1}$$

where g is the gravitational acceleration, $\Delta\rho$ and ρ_0 are the density anomaly and a reference density, respectively, f the Coriolis parameter, and H the thickness of the buoyant coastal layer. It should be noted that M represents the baroclinic part of the volume flow, i.e., the flow occurring mainly on the seaward side of the isobath where the layer of light water reaches down to the bottom. Inside this isobath a barotropic flow of buoyant water may occur along the topography.

b. The problem under consideration—buoyancy variation along the coast

In most situations, the upper-ocean density varies along the coast. In Kattegatt off the Swedish west coast, for example, the freshwater-diluted coastal current entrains more saline water along its path (Rodhe, 1998). The entrainment implies that the volume transport should increase downstream, despite the decreasing density anomaly of the buoyant layer. The warm Atlantic water penetrating into the Nordic Seas, on the other hand, is modified along its path primarily by buoyancy loss due to air-sea heat transfer (Mauritzen, 1996). Undoubtedly such variations of the properties of the buoyant layer must have dynamical consequences; see Eq. (1). In this paper we will consider the case when the buoyancy is decaying downstream due to cooling, ignoring entrainment of ambient water. Accordingly, we will focus on the situation in which a stationary solution requires that the volume transport is conserved along the flow.

Motivated by the conditions in the Nordic Seas, we consider the dynamical evolution of a buoyant current that passes over a sill in to a semi-enclosed basin. We have approached this problem with a set of numerical experiments as well as with a theoretical analysis. An important qualitative aspect of our findings is outlined in Figure 2, which illustrates that a barotropic current confined to the shelf develops as the boundary current is losing buoyancy and thereby baroclinic transport capacity along its path. As reported by Orvik *et al.* (2001), such a double-current structure is in fact a persistent and well-documented feature of the Norwegian Atlantic Current; an issue that will be further discussed in Section 4.

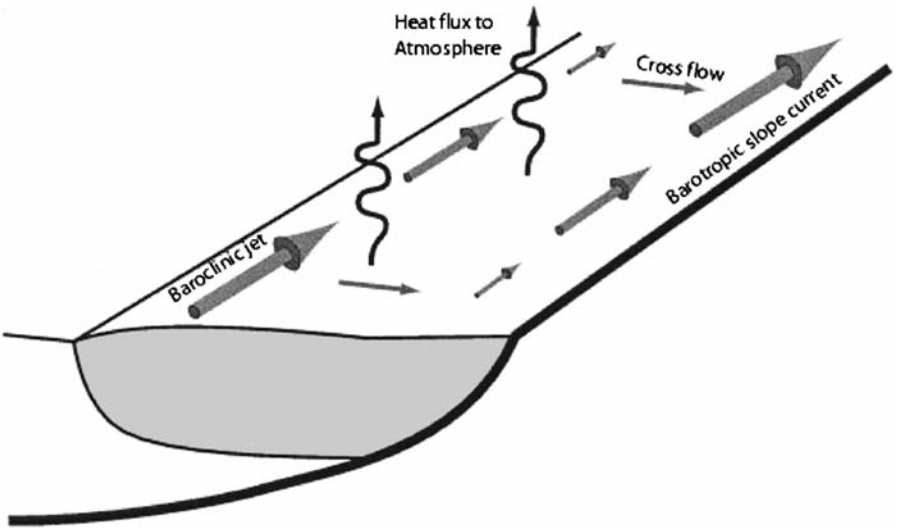

Figure 2. Illustration of the transition from a baroclinic jetstream to a barotropic slope current. Downstream decay in buoyancy is accompanied by (i) decreasing transport in the baroclinic jetstream, (ii) a flow toward the coast, and (iii) an increasing volume flow in the barotropic slope current. The total transport remains unchanged.

c. Previous related investigations

It is worth pointing out that we are particularly interested in the limiting case when all the buoyancy is extracted from the water in the boundary current. In this case, the water in the boundary current eventually becomes dense enough to serve as a source of deep water south of the sill. Viewed from this perspective, the present study concerns the branch of the thermohaline circulation where the surface water becomes dense and penetrates down into the deep ocean. Some dynamical aspects of this "sinking" branch of the thermohaline circulation have been studied by Marotzke and Scott (1999), Spall and Pickart (2001), and Spall (2003, 2004). However, the present work differs in the sense that the dynamical consequences of a sill are explored.

A recent study by Lentz and Helfrich (2002), who experimentally investigated the propagation of a buoyant gravity current along a sloping bottom, is somewhat related to the present study. Using scale analysis, they derived estimates of the propagation speed of a plume of buoyant water that emanates from a source at the coast. Behind the advancing nose of the plume, a buoyant coastal current is established. Their study demonstrates the importance of the sloping topography in that the speed of the nose is drastically reduced compared with the vertical-boundary case. It should be pointed out, however, that the study by Lentz and Helfrich (2002) primarily focuses on the transient establishment of flow on the slope, whereas the present focus is on the steady-state circulation in a large basin.

The importance of bottom friction for the structure of buoyant coastal currents on a

sloping bottom was studied by Chapman and Lentz (1994). Their results bear some relevance for our study and are commented upon in Section 3b.

d. Outline of work

In Section 2, we present results from a numerical model of an idealized system designed to capture essential properties of the Nordic Seas, including its interaction with the North Atlantic. Section 3 is devoted to a theoretical consideration related to the general problem of a surface-layer flow with buoyancy variation along a continental boundary. In the concluding section, we discuss the possible relevance of our results for the Nordic Seas.

2. A numerical model for a prototype Nordic Seas circulation

Our aim is to simulate the basic fluid dynamics of the penetration of buoyant water and the ensuing flow through a semi-enclosed basin (which would correspond to the Nordic Seas) using an idealized model. An essential feature of the model is smooth, well-resolved topography with gently sloping boundaries and a smooth sill at the entrance of the semi-enclosed basin. South of the sill, a buoyant layer should reside on top of denser deep water. North of the sill, in the semi-enclosed cold basin, heat should be lost to the atmosphere at a fairly high rate.

An obvious problem is how to create the warm layer outside the sill. In the real North Atlantic this layer is the result of complicated mixing processes, wind drift and supply of light water masses from other parts of the World Ocean; processes which are outside the scope of the present study. However, while the presence of a warm pool outside the sill is a necessary ingredient for the phenomena under consideration it may be less important how it has been created. Accordingly, we have simplified the production of this buoyant layer by relaxing the water south of the sill towards a raised temperature. Furthermore, we have reduced the ocean south of the sill to a basin of the same size and shape as the northern semi-enclosed basin. The heat loss to the atmosphere, taking place in the cold northern basin, is simulated in a straightforward way by relaxing the surface layer to a low temperature. Accordingly, the basic ingredients in our model are

1. two basins with smooth topography separated by a smooth sill;
2. a persistent production of a buoyant (warm) layer in the southern basin;
3. heat loss to the atmosphere in the northern basin.

a. Details of the model

We use the MIT ocean model (Marshall *et al.,* 1997a,b) for our simulations. The horizontal grid spacing is 25 km and the grid has 80×160 points. The model has 25 vertical levels with a spacing ranging from 50 m at the surface to 200 m at the bottom. The model uses Cartesian coordinates on an f-plane, with $f = 1.2 \cdot 10^{-4}$ s^{-1}. Horizontal and vertical viscosities are 1000 m^2 s^{-1} and 10^{-3} m^2 s^{-1}, respectively, whereas the horizontal

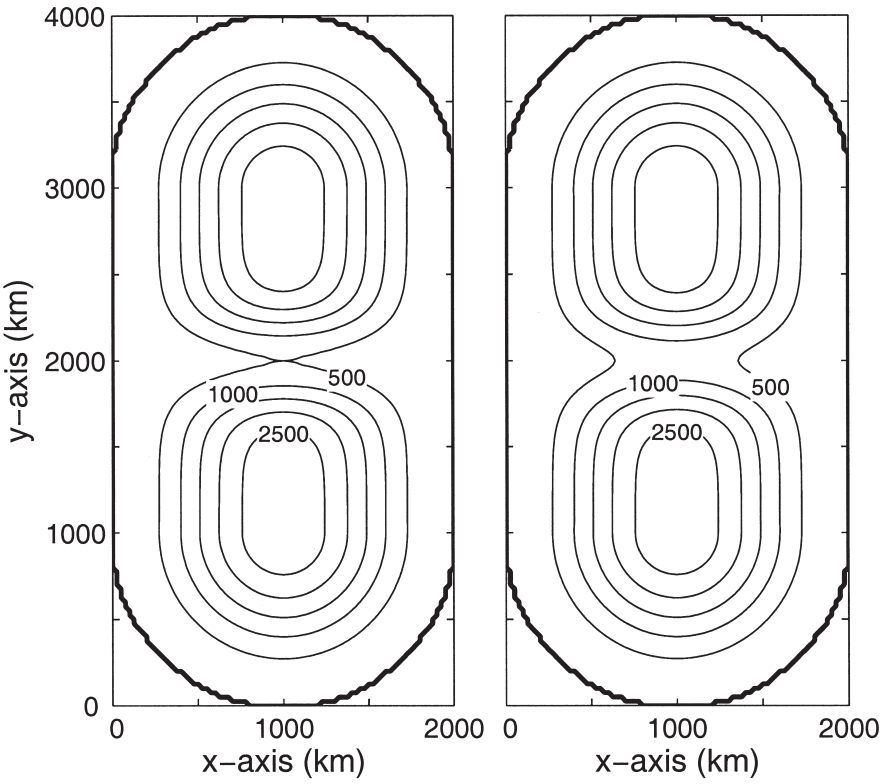

Figure 3. The bottom topography used in the numerical simulations; for the sill depths 500 m (left panel) and 700 m (right panel). Note that the heavy lines delineate the coast line. Isobaths are drawn for every 500 m.

and vertical diffusivities are $100\,m^2\,s^{-1}$ and $10^{-4}\,m^2\,s^{-1}$, respectively. The density depends only on temperature and we use a linear equation of state with a thermal expansion coefficient equal to $2 \cdot 10^{-4}\,°C^{-1}$. The time step is 50 s for the barotropic component and 600 s for the baroclinic component. The standard boundary condition on the tangential velocity is no-slip on the solid boundaries, but the results from a few simulations with free-slip conditions will also be reported below.

The model basin has two bowl-shaped parts communicating over a sill as illustrated in Figure 3. We have performed simulations with three different sill depths, namely 300, 500, and 700 m. Note that the bottom slope reaches a maximum some distance from the coast, as can be seen in Figure 7.

In the southern basin, we maintain a deep warm pool in an artificial manner: South of $y = 1000$ km and down to a depth of 1000 m, the temperature is relaxed toward 20°C; with an internal heat source given by $k(20 - T)$ where T is the instantaneous temperature. To somewhat soften this harsh forcing, the relaxation parameter k decreases linearly

northwards to zero at $y = 1000$ km. The maximum value of k corresponds to a temperature relaxation timescale of 20 days.

Cooling of the sea surface is applied north of $y = 1000$ km. Here, the surface heat flux is calculated as

$$Q = \begin{cases} a \cdot T \text{ W m}^{-2} & \text{if } T < 5°\text{C} \\ a \cdot 5 \text{ W m}^{-2} & \text{if } T > 5°\text{C}; \end{cases} \tag{2}$$

where T is the sea-surface temperature and

$$a = 95 \text{ W m}^{-2\circ}\text{C}^{-1}. \tag{3}$$

The limitation of the heat flux for temperatures over 5°C is a pragmatic way to avoid extreme cooling in the southern basin.

All our simulations have been integrated for 5000 days. The time-averaged fields discussed below represent the time mean taken over the last 2000 days of the simulation. At that stage in the integration, the flow has attained a statistically steady state.

b. Results from the simulations

In the southern basin where the heating is applied the fields do not settle to an even approximately stationary solution, while in the northern basin the fields are less variable and dominated by the mean circulation and temperature fields. Figure 4 shows an instantaneous surface temperature field, which illustrates the intense eddy activity on and south of the sill and the more organized flow north of the sill. Furthermore, near-shore eddies in the boundary current in the northern basin are clearly visible. These eddies are presumably generated in response to the more rapid cooling in the shallow region close to the shore, thus serving to even out the ensuing temperature gradient; see the studies of, e.g., Pringle (2001) and Chapman (2003) for a further discussion of cross-shelf eddy heat transports.

The flow on the sill is strongly time dependent and a detailed description is outside the scope of the present work. A visual inspection of the time-dependent flow field suggests that the penetration of warm water over the sill occurs in intermittent pulses, which involve concentrated westward flow on the southern slope of the sill and eastward flow on the other side. Probably, the flow conditions on the sill are sensitive to the details of the forcing, i.e., mainly how the warm layer is created. Below, we will describe the qualitative properties of the time-averaged fields in the northern basin, which show some interesting and presumably robust qualitative characteristics.

Figures 5–8 delineate some aspects of the time-averaged circulation. It should be noted that each of these figures presents results from two simulations with different sill depths (500 m and 700 m). On the basis of Figures 5–8, the qualitative properties of the flow in the cold, northern basin may be summarized as follows. The warm water mainly penetrates over the eastern part of the sill and flows around the norther basin as a boundary current. (We will use the term rim current to denote the boundary current that encircles the northern

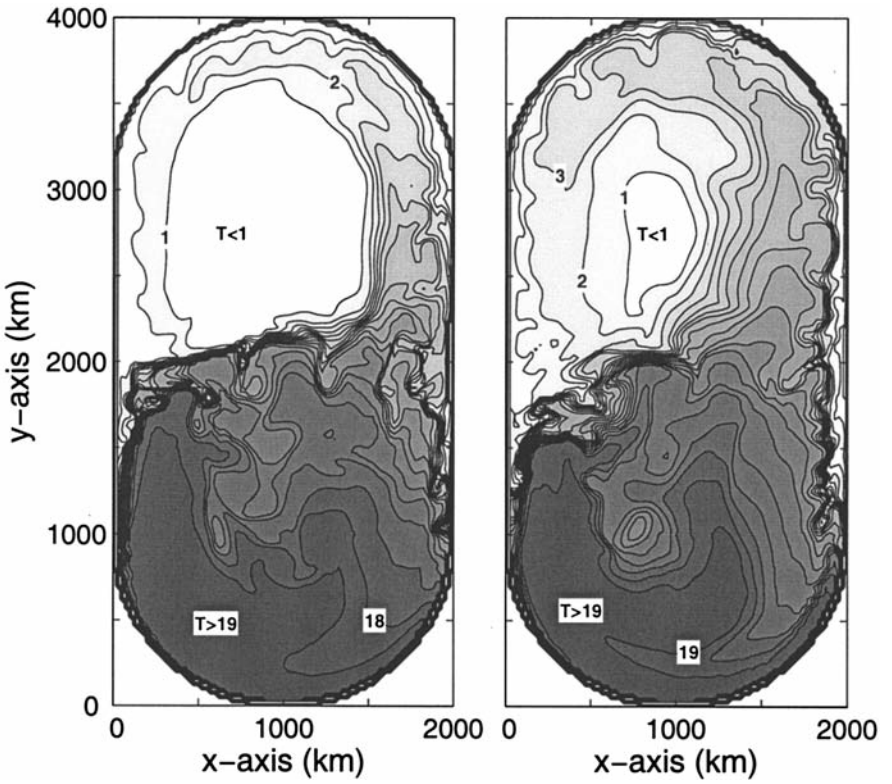

Figure 4. Instantaneous temperature fields at the sea surface; for the sill depths 500 m (left panel) and 700 m (right panel). The wiggles in the northern basin are related to eddy activity in the near shore region presumably created by the rapid cooling and associated instability in the shallow zone near the shoreline. Isotherms are drawn with a spacing of 1°C.

basin.) When the rim current enters the cold basin, its thickness is approximately equal to the sill depth. The main part of the flow initially occurs as a baroclinic jetstream flowing on top of a stagnant body of deep water. A smaller part of the warm flow is found as a barotropic current on the slope where the buoyant water reaches down to the bottom. (In what follows we use the notation "slope current" for this part of the rim current.) As the rim current proceeds around the basin losing buoyancy, its volume transport is gradually transferred from the baroclinic jet to the barotropic slope current, which exits over the sill as a cold flow.

Inspections of the numerical results show that the bulk of the water below sill depth does not take part in the circulation. (The weak anticyclonic vortex in the deep central basin, which can be seen in Fig. 8a, has no or very little relevance for the circulation in the surface layer.) An obvious consequence is that the cold flow southwards over the sill, which will contribute to the formation of deep water in the southern basin is derived from the rim

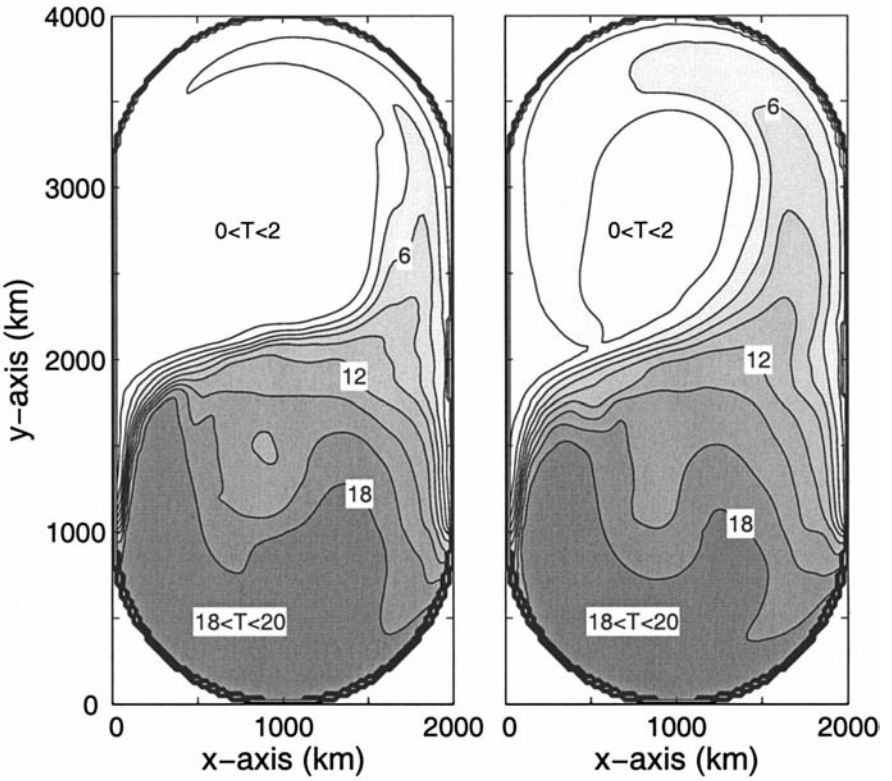

Figure 5. Time-averaged surface temperature fields; for the sill depths 500 m (left panel) and 700 m (right panel). The time averages are based on the last 2000 days in the integrations. Isotherms are drawn with a spacing of 2°C.

current (i.e., from levels at or above sill depth), rather than from the deep layers in the northern basin.

The sill depth is of primary importance for the volume and heat flow over the sill in the present simulations. A deeper sill results in a larger volume flow with higher temperature. We have estimated the volume transport and maximum temperature in the rim current when it is crossing over $y = 2500$ km on the eastern and western side, respectively. On the eastern side we obtain: The 300 m sill yields 4.5 Sv (1 Sv $= 10^6$ m^3 s^{-1}) and 7.5°C; the 500 m sill yields 19 Sv and 8.2°C; and the 700 m sill yields 54 Sv and 9.5°C. On the western side, we find the same volume transports but much lower temperatures.

The structural change of the flow from a mainly baroclinic jetstream to a barotropic slope current is demonstrated in Figures 6 and 8. In Figure 6 which shows absolute velocity at the surface, one can see how the maximum current velocity is shifted closer to the shore as the current proceeds around the basin. Figure 8 shows the presence of a stronger slope current on the western side of the basin, although the decay of the baroclinic jetstream is far from complete in the case with the deeper sill (shown in Fig. 8b).

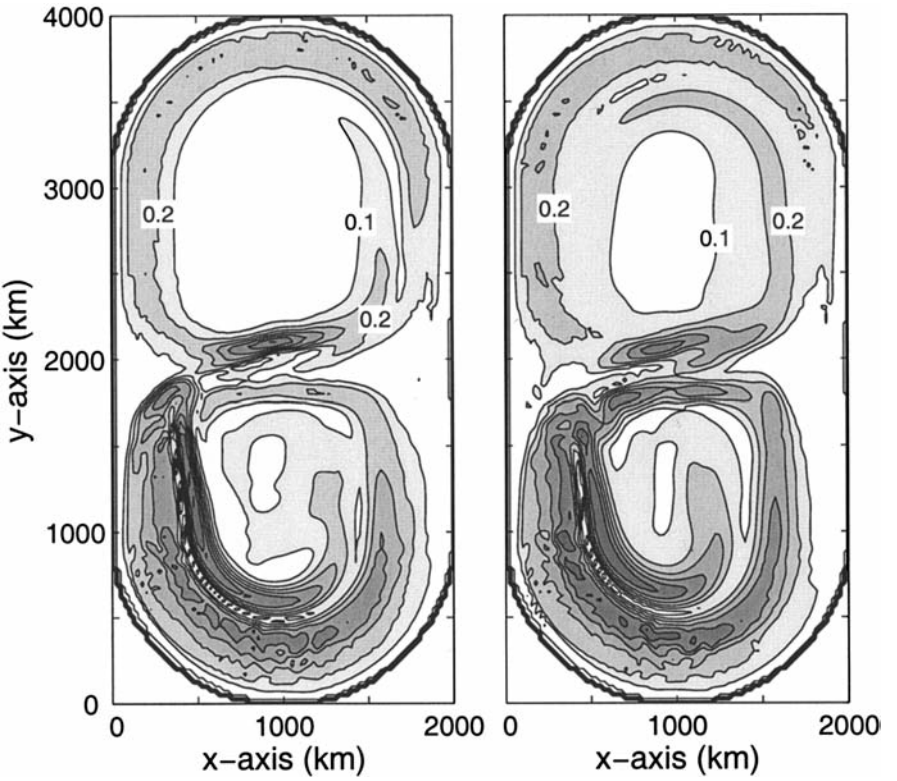

Figure 6. Time-averaged fields of the absolute current speed at the sea surface; for the sill depths 500 m (left panel) and 700 m (right panel). Note the shape of the 0.2 m s^{-1} isoline, which illustrates the transfer of the flow from the baroclinic jetstream to the barotropic slope current closer to the shore. Isolines are drawn with a spacing of 0.1 m s^{-1}.

c. Results from simulations with modified forcing and resolution

In our simulations the baroclinic inflow is transformed to a barotropic flow on the slope at relatively shallow depth. This feature makes outflow over the sill much easier in view of the potential vorticity conservation which would severely constrain deep barotropic motion. Accordingly, we believe that gently sloping boundaries are an absolutely vital ingredient for the outcome of the present simulations since they allow for the formation of a shallow barotropic flow. This has motivated us to test a couple of different smooth topographic shapes, but these modifications have not caused any basic differences in the simulated fields. Accordingly, we feel confident that the qualitative properties of the system are not sensitive to modest variations of the topographic characteristics.

In our simulations the internal Rossby radius is on the order of 20 km while our grid spacing is 25 km, indicating that the smallest baroclinic eddies may be poorly resolved in our simulations. We have repeated a simulation (sill depth 500 m) with double resolution

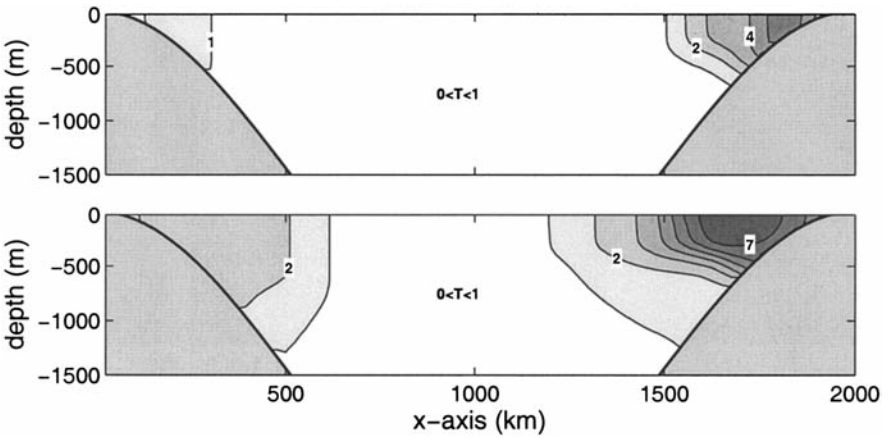

Figure 7. Time-averaged temperature field in a vertical section along $y = 3000$ km; for the sill depths 500 m (upper panel) and 700 m (lower panel). Apart from water colder than 2°C, the "Atlantic" layer remains at or above sill level. Isotherms are drawn with a spacing of 1°C.

(i.e., 12.5 km) obtaining results that are essentially similar to the reference simulation with coarser resolution. We note that the dominant eddy activity (see Fig. 4) has length scale greater than 100 km, which suggests that the present resolution should resolve the most important scales of the flow.

The present simulations have lead us to conclude that the downstream cooling is vital for

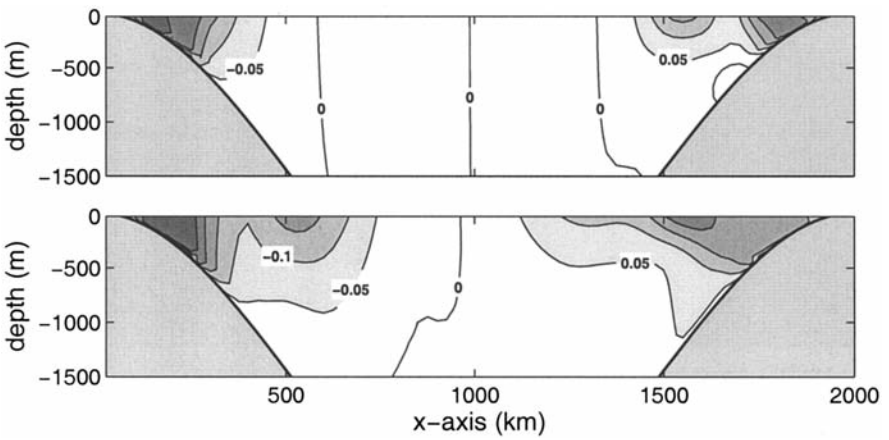

Figure 8. Time-averaged northward current in the same section shown in Figure 7; for the sill depths 500 m (upper panel) and 700 m (lower panel). Water in the central part of the basin and below the sill level is practically stagnant, except for a weak anticyclonic deep vortex in the shallow-sill case. Note that the barotropic slope current is stronger and the baroclinic jetstream weaker on the western side of the basin. Isolines are drawn with a spacing of 0.05 m s^{-1}.

the formation and downstream enhancement of a barotropic flow on the slope. A relevant question is thus how the flow will respond to a weaker cooling rate. However, it should be noted that some heat loss is a prerequisite for obtaining an exchange over the sill. Without cooling, the northern basin will soon be covered with buoyant water and the entire circulation brought to an end.

We have conducted a few simulations (sill depth 500 m) with reduced rate of cooling. By reducing the cooling rate with a factor 2, the warm water penetrates further in to the northern basin. As a result, the transfer from the baroclinic flow to the slope current occurs farther downstream, which demonstrates the connection between the downstream cooling and the enhancement of the slope current. (In fact, the sea surface temperature field appears similar to that obtained in the simulation with the standard cooling rate and a sill depth of 700 m). When the cooling rate was reduced by a factor of 8, on the other hand, the warm water tended to spread over the entire surface of the northern basin and the model did not reach a statistically steady state during the 5000-days integration.

In our standard simulations, we have used a no-slip boundary condition, i.e., with a bottom stress and an associated boundary-layer flow towards greater depth. On the shallow upper-part of the slope, we thus expect the bottom friction to have an influence on the flow field. To investigate this issue, we have performed a simulation (sill depth 500 m) with a free-slip boundary condition. We find that the free-slip condition augments the flow and increases the penetration of warm water to the extent that the thermal structure resembles the standard case with a 700 m sill. It is primarily the flow on the slope that becomes stronger, while the baroclinic part of the flow is less enhanced by the free-slip condition. Presumably, the slope current has a greater strength already when entering over the sill into the northern basin. We conclude that bottom friction, although important for the strength of the circulation, does not change the qualitative properties of the system (see also the discussion in Section 3b).

3. Theoretical considerations

This section presents some theoretical considerations regarding coastal baroclinic currents with decaying buoyancy in the downstream direction. Our first objective is to demonstrate that the total volume flow in the coastal current remains constant, despite the downstream decay of baroclinic transport capacity caused by loss of buoyancy. Our second objective is to show that the volume transport is transferred from the baroclinic jetstream to a barotropic slope current as illustrated in Figure 2. As pointed out above, the numerical simulations give rise to baroclinic eddies, hereby causing a time-dependent flow field. In the model, the eddies play an important role in the heat balance and affect the time-averaged thermal structure of the flow. However, we will show that the qualitative features of the time-averaged flow field can be deduced from the time-averaged temperature field employing elementary hydrostatic and geostrophic considerations. We will make use of the following assumptions and constraints.

1. The pressure obeys the hydrostatic law

$$\frac{\partial p}{\partial z} = -g\rho. \tag{4}$$

2. The flow field is in geostrophic balance

$$\mathbf{u} = \frac{1}{f\rho_0}\mathbf{k} \times \nabla p, \tag{5}$$

where $\mathbf{u} = (u, v)$ is the horizontal velocity and $\mathbf{k}$ a vertical unit vector.

3. The flow is assumed to be steady and to occur on an f-plane, implying that the geostrophic velocity is nondivergent. Further, the flow is taken to be inviscid, implying the absence of Ekman boundary layers. These two restrictions demand that the vertical velocity is zero everywhere. Consequently, the horizontal velocity at the bottom must either vanish or be aligned with the bottom contours:

$$\mathbf{u}_b \cdot \nabla H = 0. \tag{6}$$

Here $\mathbf{u}_b$ is the bottom-velocity and $H(x, y)$ the depth.

We will show that these dynamical assumptions suffice to explain the emergence of a slope current: In essence, the decreasing downstream buoyancy is associated with a thermal-wind flow (relative to zero velocity at the bottom) toward the coast. In principle, a barotropic flow component directed toward the central basin could cancel the shoreward thermal-wind transport. However, the assumption of a strictly geostrophic flow field disallows barotropic flow across the isobaths. Accordingly, continuity of volume requires that a decrease in downstream buoyancy is associated with an increase in the transport accomplished by the current on the slope.

We will now analyze the consequences of the above constraints on an along-shore flow with decreasing downstream buoyancy. Specifically, we consider the situation delineated in Figures 7 and 8: a baroclinic flow enters over a sill into a subpolar basin and progresses essentially along a coastline. Farther seaward, the layer of buoyant water vanishes and a homogeneous body of motionless dense water outcrops. The density field is assumed to be known and specified as

$$\rho = \rho_0(1 - q), \tag{7}$$

where ρ_0 is the deep water density and $q = q(x, y, z)$ measures the density anomaly. On the shoreward side of some isobath, say at $H = H_0$, the buoyant water reaches the sea bed. To simplify the analysis, we focus on a situation with straight coastline (aligned with the y-axis as shown in Fig. 9) where the depth H is a function of x alone. However, it is straightforward to extend the analysis to the situation with a curved coastline and a two-dimensional bottom profile.

By integrating the hydrostatic Eq. (4) we obtain

$$p = -g\rho_0 z + g\rho_0 \int_{-H(x)}^{z} q dz + p_0(x, y), \tag{8}$$

where $p_0(x, y)$ is an arbitrary function. Using this result in combination with the geostrophic relation (5), we arrive at

$$\mathbf{u} = \frac{g}{f} \int_{-H(x)}^{z} \mathbf{k} \times \nabla q dz + \frac{g}{f} q_H \mathbf{k} \times \Delta H + \frac{1}{f\rho_0} \mathbf{k} \times \nabla p_0, \tag{9}$$

where q_H is the density anomaly at $z = -H(x)$, i.e.,

$$q_H(x, y) = q(x, y, -H). \tag{10}$$

Eq. (9) warrants a few comments. To begin with, the first term on the right-hand side represents the thermal-wind velocity relative to zero flow at the bottom, while the two other velocity components are barotropic, i.e., constant through the water column. Further, the second term describes a flow aligned with the isobaths. Since one of our basic assumptions is that the bottom flow is aligned with the depth contours, also the flow related to p_0 must be aligned with the depth contours. This is fulfilled provided that

$$p_0(x, y) = p_0(H). \tag{11}$$

Furthermore, we assume that the deep water is stagnant (see Fig. 9), which implies that

$$p_0(H) = 0 \quad \text{when} \quad z < -H_0. \tag{12}$$

We underline that the flow under consideration is not ideal since the density is allowed to change along the streamlines in response to surface heat loss. As a consequence, the first term in Eq. (9) may yield a net cross-isobath volume transport even if there is a flow aligned with the depth contours at the bottom. We note that this would be impossible for an ideal flow in geostrophic balance.

The Eq. (9) and the condition (11) specify the velocity components (u, v) perpendicular and parallel to the coast:

$$u = -\frac{g}{f} \int_{-H(x)}^{z} \frac{\partial q}{\partial y} dz, \tag{13a}$$

$$v = v_J + v_S + v_{S0}, \tag{13b}$$

where we have introduced

$$v_J = \frac{g}{f} \int_{-H(x)}^{z} \frac{\partial q}{\partial x} dz, \; v_S = \frac{g}{f} q_H \frac{\partial H}{\partial x}, \; v_{S0} = \frac{1}{f\rho_0} \frac{\partial p_0(H)}{\partial x}. \tag{14}$$

The first term in Eq. (13b), v_J, represents a baroclinic flow vanishing at the bottom. This flow tends to be concentrated to the seaward edge of the buoyant layer where the isopycnals bend up toward the surface. We denote this flow the baroclinic jetstream; it is always flowing in the "downstream" direction (i.e., the positive y-direction).

The last term v_{S0} represents a barotropic flow on the slope which can be chosen freely, e.g., to match an upstream condition. We call this the "true" barotropic flow, since it is independent of the density field. The second term, v_S, represents a barotropic flow determined by the density anomaly $q_H(x, y)$ on the bottom. This contribution is located on the slope within the buoyant layer and is directed backward relative to the downstream direction defined by the baroclinic jet.

The barotropic flow components v_S and v_{S0} are both located on the slope. Accordingly, the total slope current v_{ST}, is given by

$$v_{ST} = v_S + v_{S0}. \tag{15}$$

Recalling that $q_H(x, y)$, by its definition, should be positive on the slope, we note that v_S is always negative. Accordingly, we find that v_{ST} will increase downstream if $q_H(x, y)$ (and hereby also v_S) decreases, e.g., as a result of heat loss to the atmosphere.

The flow perpendicular to the isobaths given by Eq. (13a) shows up when $q(x, y, z)$ varies along depth contours. If $q(x, y, z)$ decays downstream, the flow will be directed toward the coast causing a transfer from the baroclinic jetstream to the slope current.

Let us now proceed to demonstrate that the volume transport in the coastal current is conserved along the coast and, consequently, that the decreasing volume transport in the baroclinic jet associated with the first term in Eq. (14) is fully compensated for by an increasing volume transport on the slope. For this purpose, we define the volume transports

$$(M_J, M_S, M_{S0}) = \int\int (v_J, v_S, v_{S0})dA, \tag{16}$$

where the integration covers the entire cross-section area of the buoyant layer. Evaluating these integrals, we obtain (as detailed in the Appendix)

$$M_J = \frac{g}{f}\int_0^{H_0} q_H(y, H)H\, dH, \tag{17a}$$

$$M_S = -\frac{g}{f}\int_0^{H_0} q_H(y, H)H\, dH, \tag{17b}$$

$$M_{S0} = \frac{1}{f\rho_0}\int_0^{H_0} p_0(H)dH, \tag{17c}$$

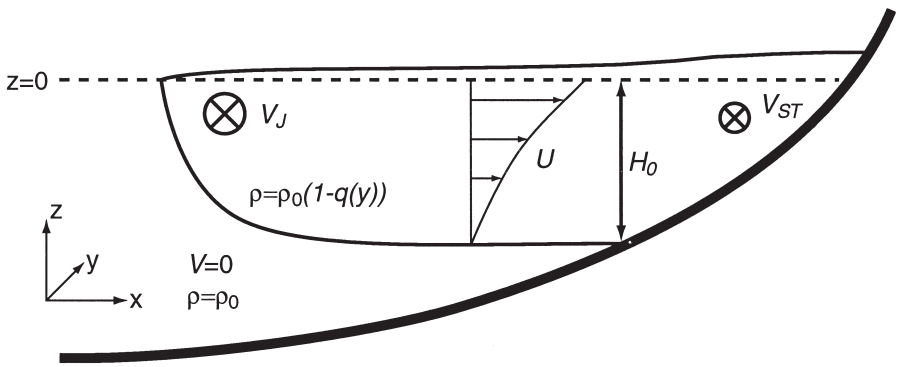

Figure 9. The "simple case" considered in Section 3a. The density in the buoyant layer depends only on the downstream coordinate y. The cross-stream flow U transfers water from the baroclinic jetstream (velocity v_J and volume transport M_J) to the barotropic slope current (velocity v_{ST} and volume transport + M_{S0}).

where it should be recalled that q_H is the density anomaly evaluated at the bottom[4] and that H_0 represents the depth beyond which q_H becomes zero. Recalling that M_{S0} by definition is constant along the coast, though otherwise arbitrary, we find that Eqs. (17) demonstrate the conservation of the along-shore transport; the total volume transport is clearly conserved since the variation of M_J will automatically be compensated by a corresponding change in M_S.

It should be underlined that the Eqs. (17) do not give any information regarding the physical location of M_J and M_S. However, it follows from the definitions given by Eq. (14) that M_S is entirely located on the slope where q_H is nonzero, i.e., at a depth smaller than H_0. On the other hand, contributions to M_J arise anywhere in the buoyant layer where the isoterms are inclined. However, in the present simulations as well as in the Svinøy section off Norway (Orvik *et al.,* 2001), the main contribution to M_J comes from the seaward side of the isobath H_0, where the isoterms bend steeply towards the surface and, as a consequence, the horizontal density gradients are large.

a. A simple case

Let us for illustrative purposes consider the simple case when the density anomaly depends only on y; see Figure 9. From Eq. (17), we obtain the following expression[5]

$$M_J = \frac{g}{2f} H_0^2 q(y), \tag{18}$$

4. Note that q_H is strictly a function of x and y as stated in Eq. (10). However, if the depth H varies monotonically approaching the shoreline, q_H may also be described as a function of y and H. For simplicity, we assume here that H has this property.

5. This formula is identical to Eq. (1), but with the density anomaly depending parametrically on y.

showing that flow in the baroclinic jet decreases with $q(y)$. This decline in the alongshore transport in the jet is balanced by a shoreward transport: Making use of Eq. (13a), we obtain

$$U = \int_{-H_0}^{0} u dz = -\frac{g}{2f} H_0^2 \frac{\partial q(y)}{\partial y}, \tag{19}$$

where U is the shoreward volume transport (per unit length) evaluated where $H = H_0$. We note that

$$U = -\frac{\partial M_J}{\partial y},$$

as required by continuity.

To specify the whole flow, we assume for simplicity that the slope current vanishes at some upstream location (say $y = 0$), i.e., the entire volume transport is accomplished by the baroclinic jet at this point. Making use of this "upstream" boundary condition, Eq. (14) predicts that the flow on the slope obeys

$$v_S + v_{S0} = -\frac{g}{f} \frac{\partial H}{\partial x} [q(0) - q(y)], \tag{20}$$

while the volume transport on the slope is given by

$$M_{S0} + M_S = \frac{g}{2f} H_0^2 [q(0) - q(y))]. \tag{21}$$

These expressions explicitly show how the flow is shifted over from the baroclinic jet to the slope current if $q(y)$ decays with y. We note that the strongest current on the slope is located where the bottom is steepest.

b. Quantitative comparison between theory and numerical simulations

The assumption of a flow in geostrophic balance is an essential ingredient in the present analysis of the slope-current dynamics. It should be recalled, however, that the numerical simulations are time dependent, exhibiting a rather strong eddy activity. Thus, it is not clear that the time-mean velocity fields in the simulations obey geostrophic dynamics even at leading order. Furthermore, the theoretical analysis assumes an inviscid flow. Accordingly, a more quantitative comparison between the simulations and our simple theoretical picture of the slope-current dynamics is called for.

To begin with, we take the time-mean velocity fields from simulations with a surface cooling-rate of 95 W m^{-2} °C^{-1} and a sill depth of 500 m. Note that we consider two different simulations: One with no-slip and one with free-slip bottom boundary conditions. In a cross section in the northern basin (located at $y = 3000$ km, see Fig. 3), we calculate the simulated net along-shore transport between the coast and an isobath H on both sides of

Table 1. Volume transports in simulations with a surface cooling-rate of 95 W m^{-2} °C^{-1} and a sill depth of 500 m; the left/right values refer to no-slip/free-slip bottom boundary conditions. Here, M_a and M_b are alongshore volume transport shoreward of the isobath H at $y = 3000$ km on the eastern and western side of the basin, respectively. ΔM_q is the diagnosed cross-isobath volume transport due to thermal-wind flow relative to the bottom. All transports are measured in units of Sverdrup.

H (m)	M_a (Sv)		M_b (Sv)		$M_b - M_a$ (Sv)		ΔM_q (Sv)	
110	0.6	1.0	0.8	1.6	0.2	0.5	0.5	0.6
280	3.7	5.2	4.4	6.8	0.7	1.6	2.9	3.2
510	7.9	11.6	10.3	14.6	2.3	3.0	5.7	5.5
690	9.4	16.1	13.9	19.1	4.5	3.0	6.3	2.4
900	10.7	21.3	16.8	22.9	6.1	1.6	6.2	0.6
1340	16.7	31.3	21.6	31.4	4.8	0.1	5.7	0.7

the basin. (We use the labels a and b to denote the eastern and the western positions on the depth contour H, respectively.) Table 1 presents the calculated volume transports (say M_a and M_b) on the eastern and the western side of the basin. We note that there is a systematic downstream increase in the volume transport occurring shoreward of the same isobath. This is in qualitative agreement with the idea that the transport is shifted from the seaward baroclinic jet to the near-shore slope current.

However, the theoretical considerations provide the following quantitative prediction: The downstream increase in transport should be equal to the shoreward thermal-wind transport crossing the isobath H between the points a and b. In other words, the increase in the flow on the slope should be directly related to the downstream decrease in buoyancy. The shoreward thermal-wind transport is obtained by integrating Eq. (13a) over the vertical surface connecting a and b, which yields (see the Appendix)

$$\Delta M_q(H) = -\frac{g}{f}\int_{-H}^{0} z(q_a - q_b)\mathrm{d}z, \tag{22}$$

where q_a and q_b are the density anomaly at the upstream and the downstream end of the segment, respectively.

To make a quantitative comparison, we take the time-mean density field from the simulations and calculate the shoreward thermal-wind transport $\Delta M_q(H)$ according to Eq. (22). The result is presented in Table 1. If the time-mean velocity field in the numerical simulations were strictly geostrophic, we would find that $\Delta M_q = M_b - M_a$. Table 1 shows that the calculated ΔM_q generally overestimates the downstream increase in transport, indicating that non-geostrophic effects give rise to an offshore transport in the model. We note that the agreement between the theoretical predictions and the numerical results is somewhat better when the free-slip conditions are employed.

Furthermore, Table 1 allows us to roughly quantify the deviation from geostrophic

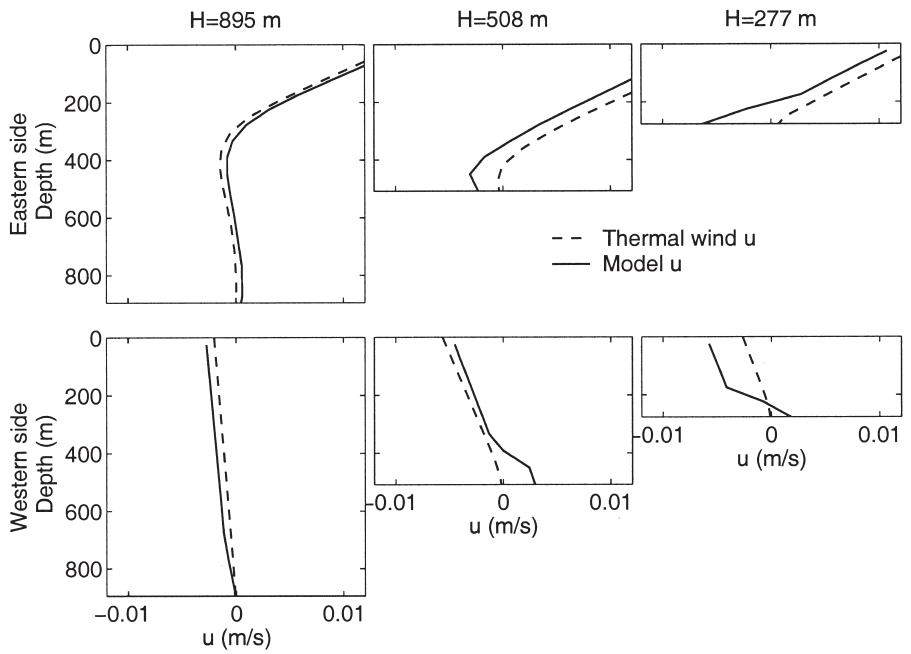

Figure 10. The cross-slope velocity (at $y = 3000$ km) in a simulation with a sill depth of 500 m and no-slip boundary conditions. The solid curve shows the simulated velocity while the dashed curve is calculated from the density gradient with aid of the thermal wind relation (13a). Deviations from a strict geostrophic balance shows up as a barotropic cross-slope component (i.e., the flow does not vanish at the bottom) as well as a boundary-layer flow near the bottom. Note that positive values means flow toward the coast on the eastern side and away from the coast on the western side.

balance in the simulations. Schematically the time-averaged momentum equation in the along-shore direction can be written as

$$f\bar{u} = -g \int_{-H}^{z} \frac{\partial \bar{q}}{\partial y}\, dz + \bar{R}, \tag{23}$$

where the overbar denotes the time average and $\bar{R}$ represents all other terms, including nonlinear and frictional effects. The fact that ΔM_q tends to be greater than $M_b - M_a$ shows that the effects represented by $\bar{R}$ tend to counteract the pressure drop due to the downstream buoyancy decrease, thereby reducing the shoreward volume transport. From Table 1, we conclude that, averaged along the depth contours, the baroclinic pressure gradient is about twice as strong as $\bar{R}$. Clearly, ageostrophic effects are significant in the present simulations. Nevertheless, our geostrophic considerations qualitatively capture many aspects of the simulated flow, as borne out in Figures 6 and 8. This view is further corroborated in Figure 10, showing the shoreward velocity as a function of depth together

with the thermal-wind flow computed from the simulated density field. As illustrated, the thermal wind relation provides a good description of the vertical shear except in the bottom boundary layer.

The difference in flow strength between the no-slip and the free-slip cases (see Table 1) shows that the bottom Ekman layer has a significant impact. As discussed by Chapman and Lentz (1994), the bottom boundary layer has a considerable influence on the structure of the density field on the slope. The Ekman layer under a buoyant coastal current generally transports water down the slope. According to Chapman and Lentz, this tends to deepen the buoyant layer and to steepen the front. Furthermore, the front tends to be pushed out to a depth great enough for the along slope current to vanish at the bottom. This tendency to deepen the buoyant structure presumably explains part of the tendency of the slope current in our simulations to migrate to a somewhat greater depth than predicted by our geostrophic analysis.

c. The role of sloping side boundaries

We believe that the sloping bottom topography is instrumental for the dynamics of the boundary current in the present numerical simulations. In particular, two features of the flow appears to depend crucially on the presence of sloping topography: The confinement of the rim current to depths shallower than the sill; and the lowest order geostrophic balance in the flow. To illuminate this issue, it is instructive to briefly consider the dynamical consequences of vertical side boundaries. Specifically, we focus on a baroclinic rim current—attached to a vertical wall at $x = 0$—flowing above a deep layer of motionless water. To the extent that geostrophy is valid, the volume transport of the rim current (say M) is given by

$$M = -\frac{g}{f}\int_{-\infty}^{0} zq(0, y, z)\mathrm{d}z,$$

where $q(0, y, z)$ is the density anomaly at the vertical boundary.[6] To conserve the volume transport in this case, the baroclinic flow must become deeper as its buoyancy decreases. In contrast, the presence of a sloping bottom allows for the development of a barotropic transport, which relaxes the constraint on the baroclinic flow to increase its thickness.

The view that sloping boundaries may serve to limit the depth of baroclinic flows is further corroborated by the numerical simulations reported by Winton (1997) and Park and Bryan (2000), who considered buoyancy-driven flows in a one-hemisphere basin with a flat bottom and a bowl-shaped geometry, respectively. In the former case, the meridional overturning extended to the bottom, while the overturning was considerably more shallow in the case where the bowl-shaped geometry was employed.

6. This expression is obtained by integrating v_J [Eq. (14)] over the whole buoyant layer seaward of the vertical wall.

It should further be pointed out that the presence of a vertical wall, in general, makes it necessary to invoke a viscous boundary layer (or some other ageostrophic effects) to satisfy the condition of zero normal flow. The basic problem is that the thermal wind relation implies that horizontal density variations along the wall (which must arise as the buoyancy declines and the flow deepens) are associated with flows perpendicular to the wall. In fact, numerical simulations reported by Spall (2003) indicate that thermohaline flows in flat-bottom basins are sensitive to the nature of the small-scale mixing that occurs near vertical boundaries (see also Spall, 2004). In contrast, the present investigation suggests that buoyancy-driven flows in basins with sloping boundaries are, to the lowest order, governed by inviscid geostrophic dynamics. Accordingly, sloping boundaries should serve to reduce the sensitivity of the large-scale flow on the details of the small-scale boundary mixing.

4. Discussion

In Section 2 we have presented simulations of the flow that results when warm water penetrates over a sill into a basin which is losing heat to the atmosphere. We found that a buoyant boundary current arises in the colder northern basin and that this current develops into a barotropic slope current located on and above sill level. In the numerical simulations, the transport in the boundary current remains constant around the basin despite the loss of buoyancy. When the current has proceeded around the entire basin, the flow exits over the sill and sinks in the southern basin. Accordingly, the deep water in the cold basin is not involved in the circulation. Our theoretical analysis suggests that the behavior of the numerically simulated boundary currents can be understood on the basis of geostrophic dynamics. We believe that our results have some relevance for the Nordic Seas which will be discussed below.

a. Relevance for the Nordic Seas

The conditions in the Nordic Seas, in particular the northward transport of relatively warm Atlantic water and the formation of deep water, have recently received a great deal of attention (cf. Hansen and Østerhus, 2000, for an overview). A main reason is that several climate-oriented studies have suggested that the inflow of Atlantic water to the Nordic Seas will decline in response to an anticipated global warming (cf. Rahmstorf, 2000; Hansen *et al.,* 2001). We will now give a brief description of the circulation in the Nordic Seas, emphasizing similarities and differences with the circulation in our idealized numerical model.

In the eastern North Atlantic, relatively warm and buoyant water extends down to depths well below the sill level of the Greenland-Scotland Ridge. In the central Nordic Seas, on the other hand, the water column is only weakly stratified. Assuming pressure equilibration at, or somewhat above, the sill level we find that the free surface will stand higher south of the sill than in the central Nordic Seas. This pressure difference is most likely a prerequisite

for the penetration of warm Atlantic water into the Nordic Seas, though other forcing mechanisms such as the wind may also be of importance.

North of the sill the Atlantic water, having a temperature of about 7°C, forms a layer with a thickness apparently set by the sill depth. Despite having a somewhat higher salinity than the deep layers underneath, this surface layer has a density deficit relative to the deep water in the range 0.2–0.6 kg m^{-3}. On the western flank of the Atlantic layer, the dense water outcrops which—in accordance with the thermal wind relation—gives rise to a frontal jet located where the isotherms bend towards the surface. As the flow proceeds northward in the Norwegian Sea, the buoyancy of the Atlantic water successively decreases as a consequence of heat loss to the atmosphere.

In a recent work Orvik *et al.* (2001) present observations of the northward flow of Atlantic water in the Svinøy section, which is located somewhat north of Bergen; see Figure 1. These observations, which cover the entire east-west extent of the Atlantic layer, show convincingly that the flow at this location has two branches: One baroclinic jetstream at the northwestern edge of the warm layer; and one barotropic current on the slope where the warm layer reaches down to the bottom. The latter, inner branch is known as the Norwegian Slope Current. According to current-meter observations, the volume transports in the two branches are roughly equal in the Svinøy section.

Qualitatively, the observed two-branch flow in the Svinøy section is strikingly similar to the current structures obtained in the present numerical simulations. Furthermore, our theoretical considerations suggest that the northward decrease in buoyancy of the Atlantic layer should give rise to a slope current. It would be interesting to investigate, on the basis of observations, whether the transport in the Norwegian Slope Current increases northward—as our results would suggest. In this context, it should be mentioned that the Norwegian Slope Current to some extent is a continuation of a current that can be traced southward on the continental slope off the British Isles (e.g., McCartney and Mauritzen, 2001). In principle, the existence of a slope current south of the Greenland-Scotland Ridge could also be attributable to the general northward decrease of upper-ocean buoyancy. Thus, an interesting question for further research would be to analyze to what extent the present results are relevant for the dynamics of the slope current in the eastern North Atlantic.

The southward flow over the sill manifests itself dramatically in the Faroe Bank Channel and in the Denmark Strait (Hansen and Østerhus, 2000). These outflowing water masses are slightly denser than the Atlantic deep water and consequently penetrate downward on the southern side of the sill. A frequently proposed point of view is that the forcing of the entire circulation, i.e., the inflow of warm Atlantic water and outflow of dense water, is dependent on the production of the particularly dense water which is observed to exit, e.g., in the Faroe Bank Channel (Hansen and Østerhus, 2000; Hansen *et al.,* 2001). As a consequence, a great deal of interest and scientific activity has been devoted to the so called deep water production, i.e., formation of water masses dense enough to renew the deepest layers in the Nordic Seas.

Based on the present idealized study, we propose a slightly modified view of how the circulation in the Nordic Seas is driven: The inflow of light Atlantic water as well as the outflow of dense water is powered by the available potential energy associated with the density contrast over the sill. Inside the Nordic Seas, a rim current connects the inflow and the outflow. We thus imagine the Nordic Seas as being filled up by a mainly homogeneous water mass, except for a coastally attached Atlantic layer. While flowing through the basin as a rim current, the Atlantic water is cooled and gradually attains the same properties as the bulk volume. The outflow emerges as a barotropic slope current—shallow enough to pass over the sill—which proceeds down into the deep Atlantic. We note that similar ideas regarding the recruitment of the outflowing water has been presented by Mauritzen (1996).

b. Some remaining challenges

In our simulations, we have used an idealized topography that is smooth and regular. It is possible that the smooth model bathymetry serves to pave the way for the flow around the basin. It remains to be explored how a more realistic topography, which should be rough and convoluted, would alter the circulation patterns obtained in the present numerical simulation. It deserves to be pointed out that topographic features in the deep parts of the Nordic Seas appear to guide some of the northward flowing Atlantic water into the central basin; an aspect of the circulation that was described already by Helland-Hansen and Nansen (1909) and has recently been analyzed from a theoretical standpoint by Nøst and Isachsen (2003). However, we note that strong cyclonic slope currents are observed in the Nordic Seas as well as in the Arctic Basin (cf. Rudels *et al.,* 2000; Nøst and Isachsen, 2003).

The dramatic outflow phenomena observed in the Faroe Bank Channel and in the Denmark Strait may give the impression that these flows are critically dependent on the very high density of the participating water masses. However, it is a challenging question whether slight changes in the water mass properties would alter the flow significantly; the hydrographic structure may be different but not necessarily the rate of flow.

In the present study, we have ignored two important aspects of the buoyancy forcing, namely its annual cycle and the salinity variations created by surface freshwater fluxes. These two effects are presumably responsible for the seasonal stratification as well as the weak mean stratification in the central Nordic Seas. In our numerical simulations, we noted that the bulk of the water and in particular the deep water is not involved in the circulation. It is a challenge to assess how this feature will change if freshwater forcing and annual variations are brought into the simulations. It should be underlined that freshwater forcing, if sufficiently strong, introduces entirely new aspects to the dynamics of thermohaline circulation: The possibility for multiple states and sudden shifts from one state to another; an idea[7] that was developed in the studies by Stommel (1961), Walin (1985), Broecker *et*

7. See Stigebrandt (1985) and Nilsson and Walin (2001) for discussions on the effects of a sill on thermohaline flows.

al. (1985), and Bryan (1986) and has subsequently been explored in climate-related research (cf. Rahmstorf, 2000).

In this context, it is worth noting that the freshwater supply to the Nordic Seas, e.g., from the Baltic, creates a coastal buoyant current of its own. Along the Norwegian coast, however, this low-saline flow is encountered near the coast and does not seem to interact significantly with the thermally dominated Atlantic current. Furthermore, the Arctic Ocean receives great amounts of freshwater which is mainly discharged as a buoyant coastal current along the east coast of Greenland. It is a great challenge to explore how this flow might interact with the rim current under consideration in the present paper.

We have also neglected the influence of wind forcing on the circulation, which undoubtedly is of great importance. In particular, the dominating cyclonic wind system serves to drive the Arctic freshwater out of the Nordic Seas along the Greenland Coast, hereby protecting the bulk water in the central basin from being too strongly diluted (Stigebrandt, 1985). Thus, a relevant extension of the present work would be to develop an idealized model for studying how buoyancy- and wind-forcing jointly drive the circulation. It deserves to be underlined, however, that our numerical simulations suggest that a reasonably strong cyclonic circulation could be maintained in the Nordic Seas even in the absence of wind forcing.

Acknowledgments. This work was supported by the Swedish Science Research Council. We further thank the Knut and Alice Wallenberg Foundation for funding the Linux Cluster "Otto" and the staff at the National Center for Super Computing in Linköping for their assistance.

APPENDIX

We here derive some volume-transport relations that are used in Section 3. We define the following transport measures

$$(M_J(x_1, y), M_S(x_1, y), M_q(x_1, y)) = \int\int_{A(x_1)} (v_J, v_S, v_q)dxdz, \tag{A1}$$

where $v_q = v_J + v_S$ and $A(x_1)$ represents the area of the cross section, spanning the entire water column, between the off-shore point $x = x_1$ and the coast ($x = 0$).

To begin, we calculate $M_J(x_1, y)$. First, we integrate v_J, defined in Eq. (14), over the entire water column. Making use of integration by parts yields

$$\int_{-H(x)}^{0} v_J dz = -\frac{g}{f}\int_{-H(x)}^{0} z\frac{\partial q(x, y, z)}{\partial x}\, dz.$$

Integrating this result from x_1 to the coast, we obtain

$$M_J(x_1, y) = -\frac{g}{f}\int_{x_1}^{0}\int_{-H(x)}^{0} z\frac{\partial q(x, y, z)}{\partial x}\, dzdx.$$

Assuming that $H(x)$ is a monotonic function, this area integral can be rewritten as

$$M_J(x_1, y) = -\frac{g}{f}\int_{-H(x_1)}^{0}\int_{x_1}^{x_2(z)} z\,\frac{\partial q(x, y, z)}{\partial x}\,dxdz,$$

where $x_2(z)$ is defined by $z = -H(x_2)$. Performing the integration with respect to x yields

$$M_J(x_1, y) = -\frac{g}{f}\int_{-H(x_1)}^{0} z[q(x_2, y, z) - q(x_1, y, z)]dz.$$

We note that $q(x_2(z), y, z) = q_H(x, y)$, where q_H is defined by Eq. (10). Using the fact that H is assumed to be a monotonic function, we can integrate the term zq_H using H as an independent variable:

$$M_J(x_1, y) = \frac{g}{f}\int_{0}^{H(x_1)} q_H(y, H)H\,dH + \frac{g}{f}\int_{-H(x_1)}^{0} zq(x_1, y, z)dz. \tag{A2}$$

Next, we consider $M_S(x_1, y)$. Integrating the velocity component v_S [Eq. (14)] vertically yields

$$v_S \cdot H = \frac{g}{f}\,q_H\,\frac{\partial H}{\partial x}\,H,$$

thus we obtain

$$M_S(x_1, y) = \frac{g}{f}\int_{x_1}^{0} q_H\,\frac{\partial H}{\partial x}\,Hdx.$$

Since

$$\frac{\partial H}{\partial x}\,dx = dH,$$

we can write

$$M_S(x_1, y) = -\frac{g}{f}\int_{0}^{H(x_1)} q_H(y, H)H\,dH. \tag{A3}$$

Note that the Eqs. (17a) and (17b) are obtained from (A2) and (A3) in the limiting case when $x_1 = -\infty$.

Finally, we consider $M_q(x_1, y)$ associated with the entire flow due to the buoyancy anomaly q. Since $M_q(x_1, y) = M_J(x_1, y) + M_S(x_1, y)$, (A2) and (A3) yield

$$M_q(x_1, y) = \frac{g}{f}\int_{-H(x_1)}^{0} zq(x_1, y, z)dz. \tag{A4}$$

Note that if the isopycnals are horizontal in the region $x_1 < x < 0$ [i.e. $q(x, y, z) = q_H(x, y)$], then $M_q(x_1, y) = M_S(x_1, y)$. In this case the flow M_J is entirely located on the seaward side of $x = x_1$. Note furthermore, that by integrating Eq. (13a) we find that the net shoreward volume transport between two points on the same isobath (say $y = a$ and $y = b$) is given by $M_q(x_1, b) - M_q(x_1, a)$.

REFERENCES

Broecker, W. S., D. M. Peteet and D. Rind. 1985. Does the ocean-atmosphere system have more than one stable mode of operation? Nature, *315,* 21–26.

Bryan, F. 1986. High-latitude salinity effects and interhemispheric thermohaline circulations. Nature, *323,* 301–323.

Chapman, D. C. 2003. Comment on "Cross-shelf eddy heat transport in a wind-free coastal ocean undergoing winter time cooling," by J. M. Pringle. J. Geophys. Res., *108(C2),* 3026, doi:10.1029/2001JC001286.

Chapman, D. C. and S. J. Lentz. 1994. Trapping of a coastal density front by the bottom boundary layer. J Phys. Oceanogr., *24,* 1464–1479.

Hansen, B. and S. Østerhus. 2000. North Atlantic—Nordic Seas exchanges. Prog. Oceanogr., *45,* 109–208.

Hansen, B., W. R. Turrell and S. Østerhus. 2001. Decreasing overflow from the Nordic Seas into the Atlantic Ocean through the Faroe Bank Channel since 1950. Nature, *411,* 927–930.

Helland-Hansen, B. and F. Nansen. 1909. The Norwegian Sea. Report on Norwegian Fishery and Marine Investigations 2, Kristiania 390 pp.

Lentz, S. J. and K. R. Helfrich. 2002. Buoyant gravity currents along a sloping bottom in a rotating fluid. J Fluid Mech., *464,* 251–278.

Marotzke, J. and J. R. Scott. 1999. Convective mixing and the thermohaline circulation. J. Phys. Oceanogr., *29,* 2962–2970.

Marshall, J., A. Adcroft, C. Hill, L. Perleman and C. Heisey. 1997a. A finite-volume, incompressible Navier Stokes model for studies of the ocean on parallel computers. J. Geophys. Res., *102(C3),* 5753–5766.

Marshall, J., C. Hill, L. Perleman and A. Adcroft. 1997b. Hydrostatic, quasi-hydrostatic, and non-hydrostatic ocean modeling. J. Geophys. Res., *102(C3),* 5733–5752.

Mauritzen, C. 1996. Production of dense overflow waters feeding the North Atlantic across the Greenland-Scotland Ridge. Part 1: Evidence for a revised circulation scheme. Deep-Sea Res., *43,* 769–806.

McCartney, M. S. and C. Mauritzen. 2001. On the origin of the warm inflow to the Nordic Seas. Prog. Oceanogr., *51,* 125–214.

Nilsson, J. and G. Walin. 2001. Freshwater forcing as a booster of thermohaline circulation. Tellus, *53A,* 629–641.

Nøst, O. A. and P. E. Isachsen. 2003. The large-scale time-mean ocean circulation in the Nordic Seas and the Arctic Ocean estimated from simplified dynamics. J. Mar. Res., *61,* 175–210.

Orvik, K. A. and P. Niiler. 2002. Major pathways of Atlantic water in the northern north atlantic and the nordic seas toward the arctic. Geophys. Res. Lett., *29(19),* 1896, doi:10.1029/2002GL015002.

Orvik, K. A., Ø. Skagseth and M. Mork. 2001. Atlantic inflow to the Nordic Seas: current structure

and volume fluxes from moored current meters, VM-ADCP and SeaSoar-CTD observations, 1995–1999. Deep-Sea Res., *48,* 937–957.

Park, Y.-G. and K. Bryan. 2000. Comparison of thermally driven circulation from a depth-coordinate model and as isopycnal model. Part I: scaling-law sensitivity to vertical diffusivity. J. Phys. Oceanogr., *30,* 590–605.

Pringle, J. M. 2001. Cross-shelf eddy heat transport in a wind-free coastal ocean undergoing winter time cooling. J. Geophys. Res., *106(C2),* 2589–2604.

Rahmstorf, S. 2000. The thermohaline ocean circulation: a system with dangerous thresholds? Climatic Change, *46,* 247–256.

Rodhe, J. 1998. The Baltic and North Seas: a process oriented review of physical oceanography, *in* The Sea, A. R. Robinson and K. H. Brink, eds., *11,* J. Wiley and Sons, Inc., 699–732.

Rudels, B., R. D. Muench, J. Gunn, U. Schauer and H. J. Friedrich. 2000. Evolution of the Artic Ocean boundary current north of the Siberian shelves. J. Mar. Syst., *25,* 77–99.

Spall, M. A. 2003. On the thermohaline circulation in flat bottom marginal seas. J. Mar. Res., *61,* 1–25.

—— 2004. Boundary currents and water mass transformation in marginal seas. J. Phys. Oceanogr., *34,* 1197–1213.

Spall, M. A. and R. S. Pickart. 2001. Where does dense water sink? a subpolar gyre example. J. Phys. Oceanogr., *31,* 810–826.

Stigebrandt, A. 1985. On the hydrographic and ice conditions in the northern North Atlantic during different phases of a glaciation cycle. Palaeogeogr., Palaeoclimatol., Palaeoecol, *50,* 303–321.

Stommel, H. 1966. The Gulf Stream. University of California Press, Berkeley, and Cambridge University Press, London, 2nd ed., 248 pp.

—— 1961. Thermohaline convection with two stable regimes of flow. Tellus, *13,* 224–230.

Walin, G. 1985. The thermohaline circulation and the control of ice ages. Palaeogeogr., Palaeoclimatol., Palaeoecol., *50,* 323–332.

Winton, M. 1997. The damping effect of bottom topography on internal decadal-scale oscillations of the thermohaline circulation. J. Phys. Oceanogr., *27,* 203–307.

Received: *24 October, 2003;* revised: *3 May, 2004.*